Nanoscale

Accepted Manuscript

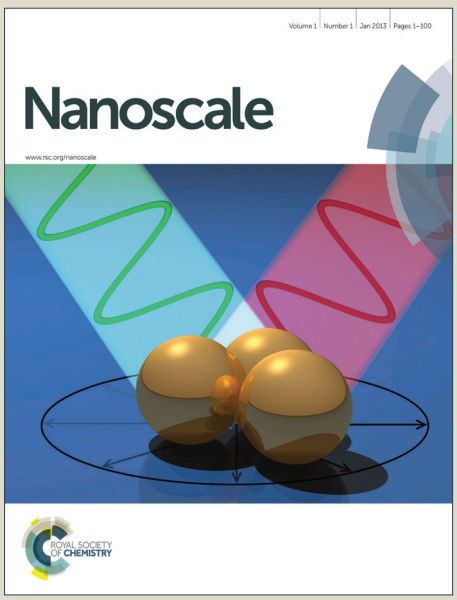

ROYAL SOCIETY OF CHEMISTRY

www.rsc.org/nanoscale

Nanoscale

RSCPublishing

COMMUNICATION

A unique hollow Li_3VO_4/carbon nanotubes composite anode for high-rate long-life lithium-ion batteries†

Cite this: DOI: 10.1039/xoxxoooooo

Qidong Li,[§] Jinzhi Sheng,[§] Qiulong Wei, Qinyou An, Xiujuan Wei, Pengfei Zhang and Liqiang Mai*

Received ooth January 2012,
Accepted ooth January 2012

DOI: 10.1039/xoxxoooooo

www.rsc.org/

A unique hollow Li_3VO_4/CNTs composite is synthesized via a facile method as an anode material in lithium batteries. Our work opens up a promising material with high rate capability and good cycle stability due to its efficient Li^+ diffusion and relatively high structure stability.

Introduction

Rechargeable lithium-ion batteries (LIBs) have been one of the most important electrical-energy storage technologies for many years, due to their high energy density, low cost and low environment impact.[1-4] In 2013, five billion LIBs had been used to supply power-hungry laptops, cameras, mobile phones and electric cars.[5] Tremendous effort has thus been devoted toward high-performance LIBs with both high-rate performance and high energy densities.[6-14] However, graphite, commercial LIBs anode material, cannot meet this high demand of the extensive development of LIBs due to its low ion conductivity (limiting the development of high-rate performance), low safety (dendritic lithium growth at low potential) and thick solid electrolyte interphase (SEI) layer (decreasing the initial coulombic efficiency).[15-19] It is urgent need to exploit a high-performance and safety anode material for the broader application of LIBs.

As a promising anode material, $Li_4Ti_5O_{12}$ has been studied as a candidate for LIBs with flat and safe potential (about 1.6 V vs. Li^+/Li), and high reversibility upon Li^+ insertion/extraction along with the negligible structure changes.[20-22] But according to $E=\Delta V\times C$ (E is the energy density, ΔV is the operation voltage of the full cell, C is capacity), the estimated energy density of $Li_4Ti_5O_{12}$ (regarding both potential and capacity) would be restricted by the relatively high potential (~1.6 V) and limited theoretical specific capacity (~160 mAh g^{-1}) when packaged full cell. Lately, $TiNb_2O_7$ with a high theoretical capacity (387 mAh g^{-1}) was reported to be an anode. The performance of $TiNb_2O_7$ has been enhanced to a high level by Guo *et al.* which showed enormous potential to be the succedaneum of graphite.[23] However its operation voltage is still high (about 1.2-1.8 V vs. Li^+/Li). Therefore, developing an anode material with both high capacity and moderate operation voltage would be significant.

Recently, Li_3VO_4 has been investigated as a hopeful intercalation anode material.[24-26] The potential of Li_3VO_4 during charge and discharge is between 0.5～1.0 V (vs. Li^+/Li), lower than that of $Li_4Ti_5O_{12}$ and $TiNb_2O_7$ but safer than that of graphite. A considerable theoretical capacity of 394 mAh g^{-1} for Li_3VO_4 is the highest among above mentioned intercalation anode materials. The Li_3VO_4 is built up of oxygen atoms in approximately hexagonal close packing, the cations occupy ordered tetrahedral sites.[27] All the octahedral sites are empty and interconnected along the c axis, forming the fast transmission pathway for Li ions. (Figure S1) All these advantages make Li_3VO_4 a promising anode for the development of high-performance LIBs. However, its low electronic conductivity results in poor electrochemical performance especially poor rate performance, preventing it from being widely used. The common method to enhance electronic conductivity is to reduce the particle size or hybridize with electronically conductive materials.[28-32] Graphene has been used by Shi *et al.* in the hollow Li_3VO_4/G composite,[26] since the hollow structure shortens ion-diffusion length while the graphene enable effective electron transport. This composite shows good cycle performance and superior rate performance, but the synthesis process is tedious. Therefore, synthesizing Li_3VO_4 with more effective architecture for the high rate performance via a facile and large-scale method remains crucial and challenging.

Herein, we present a unique hollow Li_3VO_4/carbon nanotubes (CNTs) composite synthesized by a simple, fast and high-yield hydrothermal method. The CNTs are connected to construct a three-dimensional (3D) conducting network and bound the hollow Li_3VO_4 (formed by water etching process) together. This kind of 3D hollow Li_3VO_4/CNTs composite is effective towards energy-storage materials which improve the electrical conductivity and facilitate the penetration of the electrolyte.[33] Different from previous reports with solid-state method[24-25] and long-term hydrothermal process[26], the Li_3VO_4/CNTs composite was synthesized just in two hours, and the unique hollow structure could be easily controlled during washing sample process. As an anode for LIBs, this hollow Li_3VO_4/CNTs composite shows excellent cycle performance (81.7% retention of its 2nd cycle capacity after 2000 cycles at 2 A g^{-1}) and extremely high

rate performance (240 mAh g^{-1} at high current up to 16 A g^{-1}). The low-cost raw materials, facile synthesis process and high-performance make it suitable for mass production.

Experimental Section

Sample preparation

First, 4 mmol NH_4VO_3 and 70 mmol LiOH dissolved in 60 ml deionized water. Then 70 mg hydroxylated carbon nanotubes (CNTs) were dispersed in above solution by magnetic stirring and ultrasonic. The resultant mixture was then transferred to a 100 mL Teflon lined autoclave and kept in an oven at 180 °C for 2 h. The product was washed with deionized water, anhydrous ethanol two times respectively and dried at 70 °C in a vacuum oven to get the hollow Li_3VO_4/CNTs composite. For comparison, the solid Li_3VO_4/CNTs composite was prepared using the same procedure but washed it just with anhydrous ethanol. And Li_3VO_4 was also prepared using the same procedure without hydroxylated CNTs. The Li_3VO_4/CNTs mechanical mixture was prepared by grinding Li_3VO_4 particles and hydroxylated CNTs. The mass ratio between Li_3VO_4 particles and hydroxylated CNTs is the same with the hollow Li_3VO_4/CNTs composite.

Material characterization

X-ray diffraction (XRD) data of samples were collected with a D8 Advance X-ray diffractometer, using Cu Kα radiation (λ = 1.5418 Å) in a 2θ range from 10° to 80° at room temperature. Thermogravimetry/differential scanning calorimetry (TG/DSC) was performed using a Netzsch STA 449C simultaneous thermal analyzer at a heating rate of 10 °C/min in air. Field emission scanning electron microscopy (FESEM) images were collected with a JEOL-7100F microscopy. Transmission electron microscopy (TEM) and high-resolution TEM (HRTEM) images were recorded by using a JEM-2100F STEM/EDS microscope. Raman spectra were obtained using a Renishaw INVIA micro-Raman spectroscopy system.

Measurement of Electrochemical Performance

The electrochemical properties were evaluated by assembly of 2016 coin cells in a glove box filled with pure argon gas. The working electrode was prepared by mixing the as-synthesized materials, acetylene black and carboxyl methyl cellulose (CMC) at a weight ratio of 75: 20: 5. The slurry was casted onto Cu foil and dried under a vacuum oven at 150 °C for 2 h. The loading of active materials was 1.2-1.5 mg cm^{-2}. Lithium pellets were used as the anode. The electrolyte was composed of 1 M $LiPF_6$ dissolved in ethylene carbonate (EC)/dimethyl carbonate (DMC) with a volume ratio of 1:1. For the Li_3VO_4-$LiFePO_4$ full-cell, the anode is limited and the weight ratio of the cathode and the anode is 6.3: 1. The capacity of full-cell was calculated based on the mass of the Li_3VO_4 electrode. Galvanostatic charge/discharge measurement was performed by a multichannel battery testing system (LAND CT2001A), electrochemical impedance spectroscopy (EIS) were tested with an Autolab Potentiostat Galvanostat. All the measurements were carried out at room temperature.

Results and discussion

Figure 1 illustrates the synthesis process of the Li_3VO_4/CNTs composite, ammonium metavanadate (NH_4VO_3) and lithium hydroxide (LiOH) were dissolved in deionized water as precursors. The connection between V and O in solution relates to the pH value. The vanadium exists in $V_4O_{12}^{4-}$ tetramer in a neutral solution.

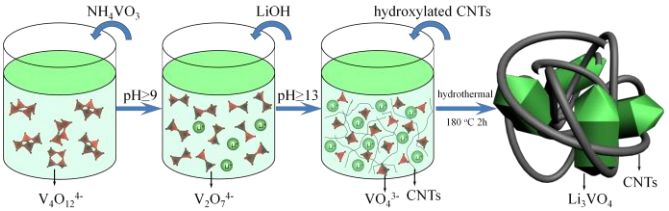

Figure 1. Schematic of the formation of Li_3VO_4/CNTs composite.

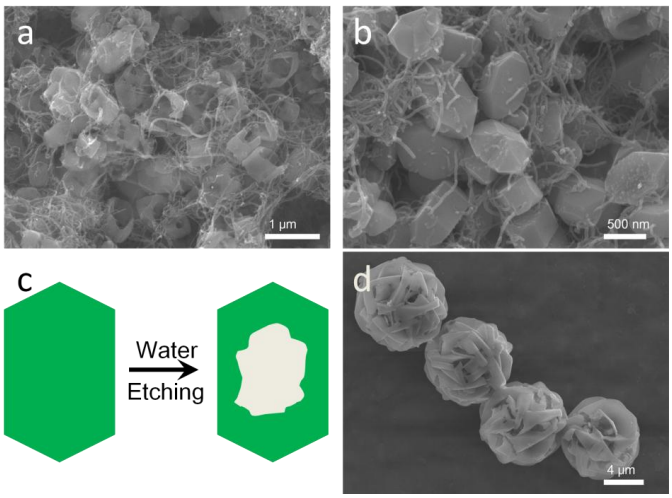

Figure 2. (a) SEM image of hollow Li_3VO_4/CNTs composite. (b) SEM image of solid Li_3VO_4/CNTs composite. (c) Schematic of water etching process from solid Li_3VO_4 particle to hollow Li_3VO_4 particle. (d) Li_3VO_4 particle without hydroxylated CNTs during synthetic process.

The $V_4O_{12}^{4-}$ tetramer will transform to VO_4^{3-} tetrahedron with the rise of pH value.[34] This process can be shown as following equation:

$$V_4O_{12}^{4-} + 4OH^- \rightarrow 2V_2O_7^{4-} + 2H_2O \ (13 \geq pH \geq 9) \quad (1)$$

$$V_2O_7^{4-} + 2OH^- \rightarrow 2VO_4^{3-} + H_2O \ (pH \geq 13) \quad (2)$$

Excess LiOH was added to make sure that the vanadium is existed in VO_4^{3-} tetrahedron. The hydroxylated CNTs were dispersed in the precursor along with ultrasonic treatment after the above substances completely dissolved. Then, the VO_4^{3-} tetrahedrons co-precipitated with Li ions to form the Li_3VO_4 particles under hydrothermal treatment. This hydrothermal reaction led to the formation of Li_3VO_4/CNTs composite with an interpenetrating network structure.

A representative SEM image of the hollow Li_3VO_4/CNTs composite is shown in Figure 2a, which exhibits hollow Li_3VO_4 particles fettered by the CNTs network. An open, screw-cap-like hollow structure can be clearly recognized in the composite. The average size of the hollow Li_3VO_4 particle is around 800 nm in length, 400 nm in width. Its wall thickness is around 50~80 nm. The solid Li_3VO_4/CNTs particles (Figure 2b) were washed with water to form the hollow Li_3VO_4/CNTs particles, which indicates that water plays crucial role in this process. Figure 2c illustrates this etching process, that the water etches the Li_3VO_4 particle from one side to the opposite side to form this screw-cap-like hollow structure. This etching process can be ascribed to selective etching process.[35] The wall thickness of the hollow Li_3VO_4 particles can be controlled by adjusting the times of washing sample as shown as Figure S3. This hollow structure is homogeneous and stable, even after the preparation of the electrode (Figure S4). The solid Li_3VO_4/CNTs particles were washed two times by water to get the hollow

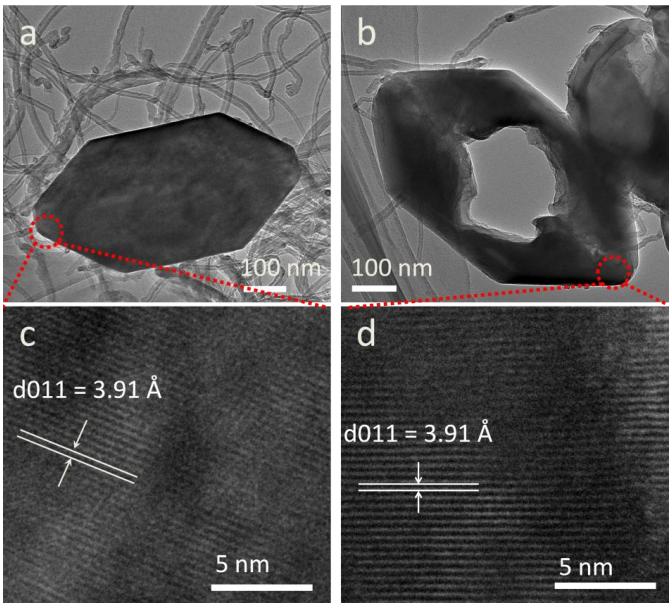

Figure 3. TEM images further confirm the etching process. (a, c) TEM and HRTEM images of solid Li_3VO_4/CNTs particle. (b, d) TEM and HRTEM images of hollow Li_3VO_4/CNTs particle.

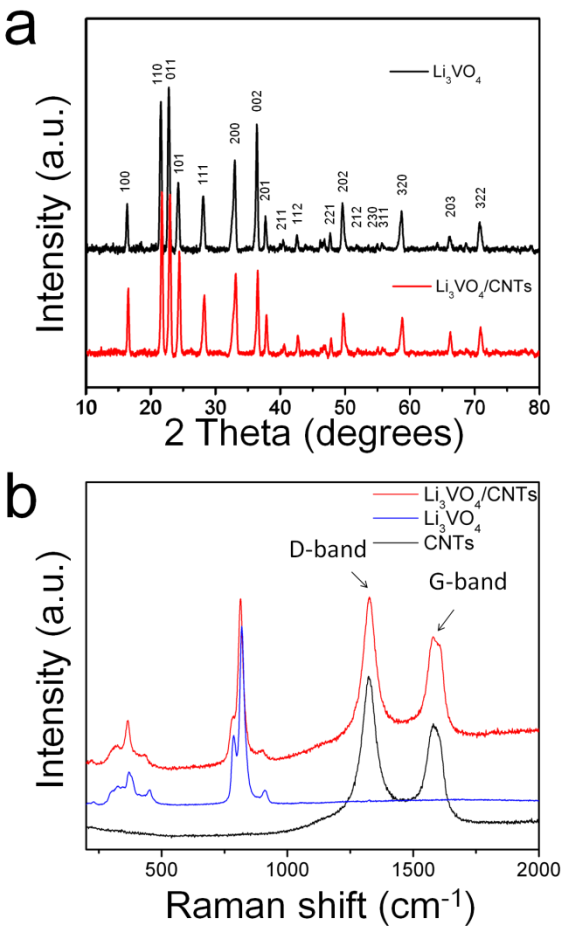

Figure 4. (a) XRD patterns of the hollow Li_3VO_4/CNTs composite and Li_3VO_4. (b) Raman spectra of the hollow Li_3VO_4/CNTs composite, Li_3VO_4 and CNTs.

Li_3VO_4/CNTs composite for considering both electrochemical performances and product production. Without the CNTs, the Li_3VO_4 particle is much bigger than the Li_3VO_4/CNTs particle, which consists of many small particles (Figure 2d). This indicates the hydroxylated CNTs not only improve the electronic conductivity but also prevent the aggregation of Li_3VO_4 particles. TEM and HRTEM were conducted to analyze the Li_3VO_4/CNTs composite shown in Figure 3a (before water etching) and Figure 3b (after water etching). The side wall thickness of the hollow Li_3VO_4 particle is about 60 nm (Figure 3b). HRTEM images (Figure 3c and 3d) taken from the front end of the particles show the clear lattice fringes with spacing of 3.91 Å, which are in agreement with the (011) plane of Li_3VO_4 (JCPDS card No. 38-1247).

Figure 4a shows the XRD patterns of Li_3VO_4 and the hollow Li_3VO_4/CNTs composite. The diffraction peaks can be well indexed to an orthorhombic Li_3VO_4 phase (JCPDS card No. 38-1247) with the lattice parameters of a = 5.447 Å, b = 6.327 Å, c = 4.948 Å, $\alpha = \beta = \gamma = 90°$, consistent to a β polymorph with space group $Pnm2_1$. Diffraction peaks which might appear for the CNTs are absent, most likely the CNTs peaks are eclipsed by that of the Li_3VO_4. Raman spectra (Figure 4b) indicate the existence of Li_3VO_4 and CNTs in the composite. The range of 280−475 cm^{-1} and 750−935 cm^{-1} represent the Li_3VO_4 bands, and the bands in the range of 1200−1460 cm^{-1} and 1470−1730 cm^{-1} are attributed to the D-band (K-point phonons of A_{1g} symmetry) and G-band (E_{2g} phonons of C sp^2 atoms) of CNTs, which confirm the existence of CNTs in the composite. The peak intensity ratio between the 1333 and 1592 cm^{-1} peaks (I_D/I_G) generally provides a useful index about the degree of crystallinity of various carbon materials, that is, the smaller the I_D/I_G ratio, the higher the degree of ordering in the carbon material.[36] The I_D/I_G value of the hydroxylated CNTs and hollow Li_3VO_4/CNTs composite is 1.375 and 1.233, respectively, indicating the enhancement of the degree of graphitization. The amount of CNTs in the hollow Li_3VO_4/CNTs composite was estimated to be approximately 13.76 wt% from the thermogravimetric analysis (Figure S5a). Our synthetic process is simple and can be easily scaled up. As a demonstration, we performed the reaction in a 500 mL autoclave with 360 mL precursor and yielded as much as ~ 3.5 g of product (Figure S5b).

Coin cells with lithium as counter electrode were used to evaluate the electrochemical performance of the as-synthesized materials. All cells were cycled between 0.2 and 3.0 V. Figure 5a shows the galvanostatic discharge (Li insertion)/charge (Li extraction) profiles for the hollow Li_3VO_4/CNTs at a low current rate of 0.1 A g^{-1}. The initial discharge capacity is 453 mAh g^{-1} (based on the total weight of the composite), higher than the theoretical capacity, because of the formation of SEI layer. A reversible capacity of 376 mAh g^{-1} can be obtained in the second discharge cycle, 83% of the initial capacity.

For practical applications (in full-cell configuration), high current delivery on demand (high rate) is very important. To evaluate the advantage of the hollow and 3D conductive structure, rate performance at progressively increased current density (ranging from 0.1 to 16 A g^{-1}) was measured (Figure 5b, c). It can be seen that the specific capacity of the hollow Li_3VO_4/CNTs composite anode are as high as 355, 273 and 265 mAh g^{-1} at 0.1, 4 and 8 A g^{-1} respectively. Even at a high rate of 16 A g^{-1}, the specific capacity is as high as 240 mAh g^{-1}, which are much higher than that of the Li_3VO_4/CNTs mechanical mixture anode (223 mAh g^{-1} at 0.1 A g^{-1}, 146 mAh g^{-1} at 4 A g^{-1}, 130 mAh g^{-1} at 8 A g^{-1} and 110 mAh g^{-1} at 16 A g^{-1}). The comparison of rate performance with previous work has been shown in Figure S10 and Table S1. For the solid Li_3VO_4/CNTs composite anode, when the current density is lower than 0.4 A g^{-1}, its capacity is approximately the same with that of the hollow Li_3VO_4/CNTs composite. But with the current density

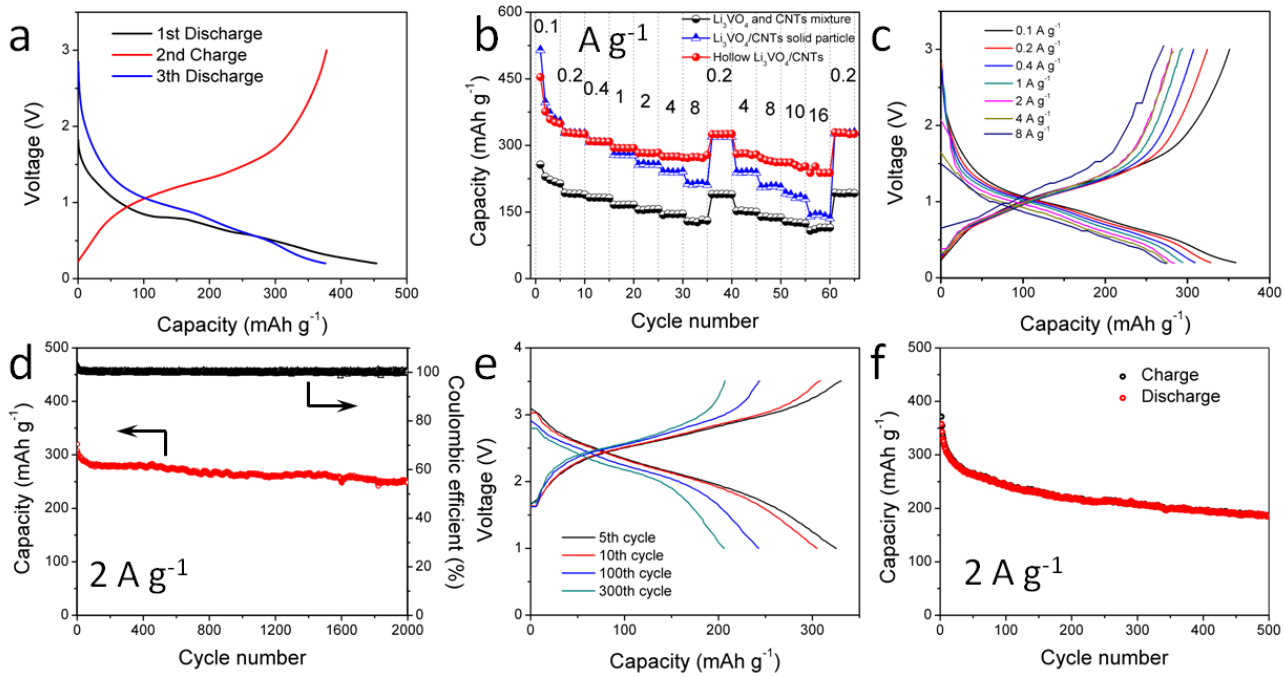

Figure 5. (a) Typical discharge/charge curves of the hollow Li_3VO_4/CNTs composite anode at a current density of 0.1 A g^{-1}. (b) Rate performance of the hollow Li_3VO_4/CNTs composite anode, the solid Li_3VO_4/CNTs composite anode, and the Li_3VO_4/CNTs mechanical mixture anode. (c) Discharge/charge curves of the hollow Li3VO4/CNTs composite anode at different current density. (d) Cycle performance of the hollow Li_3VO_4/CNTs composite at 2 A g^{-1}. (e, f) Cycle performance and typical discharge/charge curves for the $LiFePO_4$-Li_3VO_4/CNTs full cell at 2 A g^{-1} with capacity limited by Li_3VO_4/CNTs cycled between 1 and 3.5 V.

going up, the capacity gap becomes obvious. The capacity of the solid Li_3VO_4/CNTs particle is 140 mAh g^{-1} at 16 A g^{-1}, 100 mAh g^{-1} lower than that of the hollow Li_3VO_4/CNTs. At 0.1 A g^{-1}, the capacity of the hollow Li_3VO_4/CNTs is a little lower than that of the solid Li_3VO_4/CNTs composite anode, due to the decreased mass ratio of the Li_3VO_4 in the composite during the etching process. To explore the capacity contribution of CNTs in the composite, coin cells with metallic lithium as anode were assembled. The rate performance of the hydroxylated CNTs was measured at the same current density range from 0.1 to 8 A g^{-1}. (Figure S6) The specific capacities of the CNTs anode are 200 mAh g^{-1} at 0.1 A g^{-1}, 70 mAhg^{-1} at 8 A g^{-1}. Consequently, the actual capacities contribution of the hollow Li_3VO_4 can be calculated to be 393.4 mAh g^{-1} (very closed to its theoretical capacity) at 0.1 A g^{-1} and 306.8 mAh g^{-1} at 8 A g^{-1}, respectively. The detailed capacity contribution ratio of each component in the composite is shown in Figure S7. Besides excellent rate capability, the hollow Li_3VO_4/CNTs composite has superior long cycle performance at high current density. The hollow Li_3VO_4/CNTs composite shows a very good stability at 2 A g^{-1}, and 250 mAh g^{-1} is still obtained even after 2000 cycles (81.7% retention of its 2nd cycle capacity). (Figure 5d)

The electrochemical impedance spectrum (EIS) was used to provide further insights (Figure S8). The EIS spectrum shows two compressed semicircles in the high to medium frequency range of each spectrum, which describe the charge transfer resistance (R_{ct}) for these electrodes, and an approximately 45 ° inclined line in the low-frequency range, which could be considered as Warburg impedance (Z_W). After simulating the second compressed semicircle for both samples, the values of R_{ct} for the Li_3VO_4 and the hollow Li_3VO_4/CNTs electrodes after 30th cycles were calculated to be 354.5 and 24.04 Ω, respectively. This result suggests that the hollow Li_3VO_4/CNTs composite has faster kinetics for Li ions insertion/extraction.[37-39]

The high rate capability, excellent cycling stability observed for the hollow Li_3VO_4/CNTs composite can be ascribed to the interconnected 3D conductive framework and the unique hollow structure as above mentioned. First, the CNTs prevent the agglomeration of the Li_3VO_4 particles to reduce the particle size which increases the contact area between Li_3VO_4 and electrolyte.[31] Li_3VO_4 particles are wrapped by CNTs and the CNTs connect together to form a 3D conductive structure at the same time, which greatly improve the conductivity.[40-42] These promote the electrochemical performance comprehensively. Second, the unique open hollow structures provide more sites for the Li ions transportation, reduce the diffusion distance for Li ions and buffer the local volume change during Li^+ insertion/extraction, leading to high stability and good charge/discharge performance at large current density.[43] The above favorable properties clearly show that the hollow Li_3VO_4/CNTs composite is a very promising candidate for practical applications in LIBs.

Full-cells combining the commercial $LiFePO_4$ cathode with our hollow Li_3VO_4/CNTs anode have been assembled. Figure 5e shows charge/discharge curves for the Li_3VO_4/CNTs- $LiFePO_4$ full cell at 2 A g^{-1} (7 min full charge or discharge). According to their respective voltage, the full cell gives an operating voltage around 2.5 V. Its capacity is above 300 mAh g^{-1} at the first few cycles, and 185 mAh g^{-1} after 500 cycles (Figure 5f). The capacity fading of full cell is 45 % after 500 cycles, very closed to that of the commercial $LiFePO_4$ (42 %) (Figure S9). And the capacity fading of $LiFePO_4$ and the hollow Li_3VO_4/CNTs is 0.107 % and 0.0275 % per cycle, respectively, which indicate the capacity fading of full cell is limited by the commercial $LiFePO_4$.

Conclusions

The Li_3VO_4/CNTs composite is synthesized via a facile, low cost and rapid hydrothermal method. The Li_3VO_4 nanoparticle could be further etched by water, resulting in the hollow structure. The hollow Li_3VO_4/CNTs composite exhibited extremely high rate performance and long cycle life, which is demonstrated by over 2000 cycles with capacity of 250 mAh g^{-1} at 2 A g^{-1}. Even at 16 A g^{-1}, 240 mAh g^{-1} can still be obtained. These excellent electrochemical performances are attributed to the connected CNTs 3D conductive framework and the hollow structure. Meanwhile, this time-saving and easy-to-operate approach can be easily put into mass production. Furthermore, a 2.5 V full cell couple with commercial $LiFePO_4$ cathode has been assembled with good high rate performance which demonstrates its application prospect on rapid charge/discharge LIBs. Therefore, it is shown that this hollow Li_3VO_4/CNTs composite can be a promising anode material for high-performance and low-cost LIBs.

Acknowledgements

This work was supported by the National Basic Research Program of China (2013CB934103), the International Science & Technology Corporation Program of China (2013DFA50840), the Fundamental Research Funds for the Central Universities (2013-VII-028, 2014-YB-001). Thanks to Prof. C. M. Lieber of Harvard University and Prof. Dongyuan Zhao of Fundan University for strong support and stimulating discussions.

Notes and references

[a] State Key Laboratory of Advanced Technology for Materials Synthesis and Processing, WUT-Harvard Joint Nano Key Laboratory, Wuhan University of Technology, Wuhan, 430070, P. R. China. E-mail: mlq518@whut.edu.cn; Fax: +86-027-87644867;Tel: +86-027-87467595

§ These authors contributed equally to this work. All authors discussed the results and commented on the manuscript. The authors declare no competing financial interest.

† Electronic Supplementary Information (ESI) available: [The crystal structure of Li_3VO_4; SEM image of hydroxylated CNT; Li_3VO_4 was etched by different dosage water; TGA curves of Li_3VO_4 and the hollow Li_3VO_4/CNT composite; The production in one pot (360 mL) was weighed to be 3.5237 g; XRD pattern and rate performance of CNT; The capacity contribution ratio of CNTs and the hollow Li_3VO_4; EIS and phase diagram of Li_3VO_4 and Li_3VO_4/CNT after 30 cycles; ECs performance of Li_3VO_4 anode material compared with other previous works]. See DOI: 10.1039/c000000x/

1. B. Kang and G. Ceder, *Nature* 2009, **458**, 190.
2. B. Dunn, H. Kamath and J.-M. Tarascon, *Science* 2011, **334**, 928.
3. H. Wu, G. Chan, J. W. Choi, I. Ryu, Y. Yao, M. T. McDowell, S. W. Lee, A. Jackson, Y. Yang and L. Hu, *Nat. Nanotechnol.* 2012, **7**, 310.
4. H. Zhang, X. Yu and P. V. Braun, *Nat. Nanotechnol.* 2011, **6**, 277.
5. R. V. Noorden, *Nature* 2014, **507**, 26-28.
6. M. Armand , J.-M. Tarascon, *Nature* 2008, **451**, 652−657.
7. C. K. Chan, H. Peng, G. Liu, K. Mcilwrath, X. F. Zhang, R. A. Huggins, Y. Cui, *Nat. Nanotechnol.* 2008, **3**, 31−35.
8. L. J. Fu, H. P. Zhang, Q. Cao, G. J. Wang, L. C. Yang, Y. P. Wu, *Micro. Meso. Mater.* 2009, **117**, 515 – 518.
9. T. Xia, W. Zhang, J. Murowchick, G. Liu, X. B. Chen, *Nano Lett.* 2013, **13**, 5289–5296.
10. Y. S. Hu, X. Liu, J. O. Müller, R. Schlögl, J. Maier, D. S. Su, *Angew. Chem*. 2008, **48**, 210-214.
11. J. J. Xu, H. Y. Wu, F. Wang, Y. Y. Xia, G. F. Zheng, *Adv. Energy Mater.* 2013, **3**, 286-289.
12. C. Wang, W. Wan, Y. H. Huang, J. T. Chen, H. H. Zhou, X. X. Zhang, *Nanoscale* 2014, **6**, 5351-5358
13. Y. Yao, N. Liu, M. T. McDowell, M. Pasta, Y. Cui, *Energy Environ. Sci.* 2012, **5**, 7927–7930.
14. H. Wu, G. Yu, L. Pan, N. Liu, M. T. McDowell, Z. Bao, Y. Cui, *Nature Commun*. 2013, **4**, 1943.
15. S. S. Zhang, K. Xu, T. R. Jow, *J. Power Sources* 2006, **160**, 1349–1354.
16. S. S. Zheng, *J. Power Sources* 2006, **161**, 1385–1391.
17. G. J. Wang; J. Gao; L. J. Fu; N. H. Zhao; Y. P. Wu; T. Takamura, *J. Power Sources* 2007, **174**, 1109−1112.
18. H.-K. Kim; S.-M. Bak; K.-B Kim. *Electrochem. Commun*. 2010, **12**, 1768−1771.
19. D. Aurbach, B. Markovsky, I. Weissman, E. Levi, Y. Ein-Eli, *Electrochim. Acta* 1999, **45**, 67-86.
20. T. Ohzuku, A. Ueda, N. Yamamoto, *J Electrochem. Soc.* 1995, **142**, 1431-1435.
21. J. Chen; L. Yang; S. Fang; S.-i. Hirano; K. Tachibana, *J. Power Sources* 2012, **200**, 59−66.
22. E. Kang, Y. S. Jung, G. H. Kim, J. Chun, U. Wiesner, A. C. Dillon, J. K. Kim, J. Lee, *Adv. Funct. Mater.* 2011, **21**, 4349-4357.
23. B. K. Guo, X. Q. Yu, X. G. Sun, M. F. Chi, Z. A. Qiao, J. Liu, Y. S. Hu, X. Q. Yang, J. B. Goodenough, S. Dai, *Energy Environ. Sci.* 2014, DOI: 10.1039/C4EE00508B.
24. W.-T. Kim, Y. U. Jeong, Y. J. Lee, Y. J. Kim, J. H. Song, *J. Power Sources* 2013, **244**, 557-560.
25. H. Q. Li, X. Z. Liu, T. Y. Zhai, D. Li, H. S. Zhou, *Adv. Energy Mater.* 2013, **3**, 428-432
26. Y. Shi, J. Z. Wang, S. L. Chou, D. Wexler, H. J. Li, K. Ozawa, H. K. Liu, and Y. P. Wu, *Nano Lett.* 2013, **13**, 4715–4720.
27. A. R. West , F. P. Glasser , *J. Solid State Chem.* 1972 , **4** , 20.
28. Q. L. Wei, Q. Y. An, D. D. Chen, L. Q. Mai, S. Y. Chen, Y. L. Zhao, K. M. Hercule, L. Xu, A. M. Khan, and Q. J. Zhang, *Nano Lett.* 2014, **14**: 1042–1048.
29. S. Li, Y. F. Dong, L. Xu, X. Xu, L. He, L. Q. Mai, *Adv. Mater.* 2014, DOI: 10.1002/adma.201305522.
30. X. L. Ji, K. T. Lee, L. F. Nazar, *Nature Mater.* 2009, **8**, 500-506
31. W. Tang, Y. Y. Hou, X.J. Wang, Y. Bai, Y. S. Zhu, H. Sun, Y. B. Yue, Y. P. Wu, K. Zhu, R. Holze, *J. Power Sources* 2012, **197**, 330-333.
32. F. X. Wang, S. Y. Xiao, Y. Y. Hou, C. L. Hu, L. L. Liu, Y. P. Wu, *RSC Adv.* 2013, **3**, 13059-13084.
33. Z. Chen, Y. Yuan, H. H. Zhou, X. L. Wang, Z. H Gan, F. S. Wang, Y. F. Lu, *Adv. Mater.* 2013, DOI: 10.1002/adma.201303317.
34. J. Livage, *Chem. Mater.* 1991, **3**, 578-593.
35. C. H. Kuo, M. H. Huang, *J. Am. Chem. Soc.* 2008, **130**, 12815–12820.
36. X. L. Wu, L. Y. Jiang, F. F. Cao, Y. G. Guo, L. J. Wan, *Adv. Mater.* 2009, **21**, 2710−2714.

37. L. Q. Mai, B. Hu, W. Chen, Y. Y. Qi, C. S. Lao, R. S. Yang, Y. Dai, Z. L. Wang, *Adv. Mater.* 2007, **19**, 3712.
38. X. Xu, Y. Z. Luo, L. Q. Mai, Y. L. Zhao, Q. Y. An, L. Xu, F. Hu, L. Zhang, Q. J. Zhang, *NPG Asia Mater.* 2012, **4**, e20.
39. L. Q. Mai, Q. L. Wei, Q. Y. An, X. C. Tian, Y. L. Zhao, X. Xu, L. Xu, L. Chang, Q. J. Zhang, *Adv. Mater.* 2013, **25**, 2969–2973.
40. X. L. Jia, Z. Chen, A. Suwarnasarn, L. Rice, X. L. Wang, H. Sohn, Q. Zhang, B. M. Wu, F. Wei, Y. F. Lu, *Energy Environ. Sci.* 2012, DOI: 10.1039/c2ee03110h.
41. Z. Chen, V. Augustyn, X. L. Jia, Q. F. Xiao, B. Dunn, Y. F. Lu, *ACS Nano* 2012, **6**, 4319–4327.
42. Z. Chen, J. W. F. To, C. Wang, Z. D. Lu, N. Liu, A. Chortos, L. J. Pan, F. Wei, Y. Cui, Z. N. Bao, *Adv. Energy Mater.* 2014, DOI: 10.1002/aenm.201400207.
43. X. W. Lou, L. A. Archer, Z. C. Yang, *Adv. Mater.* 2008, **20**, 3987–4019.

